Nature Environment and Pollution Technology
An International Quarterly Scientific Journal

p-ISSN: 0972-6268
(Print copies up to 2016)
e-ISSN: 2395-3454

Vol. 21 | No. 2 | pp. 487-496 | 2022

Original Research Paper

https://doi.org/10.46488/NEPT.2022.v21i02.007

Open Access Journal

Hydraulic Performance and Energy Loss Effect of Pit Structure Optimized Drip Irrigation Emitter

Tianyu Xu*, Shuteng Zhi*, Qiuyue Yu and Ennan Zheng*†**

*School of Hydraulic and Electric Power, Heilongjiang University, Harbin, 150080, China

**Rural Energy and Environmental Protection Institute, Heilongjiang Academy of Agricultural Sciences, Harbin 150086, China

†Corresponding author: Ennan Zheng ; 1115291208@qq.com

Nat. Env. & Poll. Tech.
Website: www.neptjournal.com

Received: 21-06-2021
Revised: 30-07-2021
Accepted: 26-08-2021

Key Words:
PODE
Orthogonal experiment
Numerical simulation
Verification test
Regression model

ABSTRACT

The pit structure optimized drip irrigation emitter (PODE) is a novel type of irrigation emitter that may provide shunts, quick diversion, and mixed flow to maximize energy loss. To study the influence of the geometric parameters of the flow channel on the hydraulic characteristics and energy loss effect, twenty-five sets of orthogonal test schemes were established. Using numerical simulation and verification tests, the flow index and energy loss coefficient were obtained. The results showed that the flow index of the PODE was 0.4632-0.5265, and its hydraulic performance was good. The energy loss coefficient under the pressure head of 5-15 m was 510-2221, which showed that the energy loss effect was obvious. The influence order of the geometric parameters on the flow index was B>P>C>D>A, the optimal solution was $P_{0.6}D_{1.4}A_{85}B_{0.25}C_{0.12}$. The determination coefficient of the regression model based on geometric parameters and flow index was 0.85. In addition, the verification test showed that the relative error among the test value, simulated value, and estimated value were less than 5%, and the flow index can be estimated reliably. The research can provide a reference for the pre-research and evaluation of the hydraulic performance and energy loss effect of the PODE.

INTRODUCTION

Bionics is a scientific method of engineering structural innovation that imitate the structure and function of biological systems in some aspect (Koch et al. 2009, Xing et al. 2012). Plants are an indispensable and important part of the biological cycle system. Many inventions and creations are derived from the bionics of plant structure or morphology. Plant bionics has a very wide range of applications (Luo et al. 2016, Barthlott et al. 2017). Drip irrigation technology is one of the high efficient water-saving irrigation technologies in agriculture. Its main advantages are good water-saving effect, no damage to soil structure, and high irrigation uniformity (Sun & Kang 2000, Lu et al. 2018). The core component of drip irrigation technology is the drip irrigation emitter, which can effectively eliminate the excess energy at the inlet and ensure uniform flow (Li et al. 2020, Mohamed & Ahmed 2017, Wei et al. 2014).

The flow index, energy dissipation effect, and anti-clogging ability are all important factors in the drip irrigation emitter's performance. The geometry of the emitter channel structure determines the three factors of performance (Li et al. 2009, Yuan et al. 2014). Many experts have proposed novel design concepts and structural types of emitters to improve hydraulic performance (Feng et al. 2017, Guo et al. 2014, Zhang et al. 2014, Yu et al. 2018). The flow index of the fractal flow channel emitter, which was constructed using fractal theory, was between 0.49 and 0.53, significantly improving the turbulence degree of the fluid in the flow channel (Li et al. 2007). The two-way opposing channel improved energy dissipation efficiency by allowing the fluid in the channel to hedge and mix (Guo et al. 2016). The hydraulic performance of the perforated drip irrigation emitter based on a perforated plate construction was good, with a flow index of 0.47-0.51 (Xing et al. 2021). The development and use of drip irrigation emitters benefited greatly from the design of a novel emitter channel.

Based on the similarity between the drip irrigation emitter and the pit structure of the plant xylem, the optimized structure of the pit drip irrigation emitter was designed (Xu & Zhang 2019, 2020). The pit structure optimized drip irrigation emitter (PODE) was used as the research object in this article, and the numerical simulation and test were used to obtain pressure and flow rate in the flow channel, and the hydraulic performance was used to analyze the drip irrigation emitter's flow mechanism. It can: (1) obtain the flow index and the energy loss coefficient of the PODE, (2) analyze the influence of geometric parameter changes on the

performance of the PODE, and (3) evaluate the prediction model and flow characteristics of the PODE. The results provide a reference for the new bionic drip irrigation emitters and offer a deeper understanding of channel design in the drip irrigation technology.

MATERIALS AND METHODS

Flow Channel Structure Design

The PODE was designed according to the torus-margo bordered pit structure in plant xylem tracheids (Fig. 1a). Preliminary work (Xu & Zhang. 2020) found that the PODE had better working performance than the pit drip irrigation emitter (PDIE). The structure of PDIE and PODE are shown in Fig. 1b & 1c.

Numerical Simulation Model

Control Equation

The non-direct numerical simulation method was chosen to be investigated in this research. The standard k–model was found to have a lot of application in the PODE model's turbulent flow. The control equations are as follows:

$$\frac{\partial(\rho k)}{\partial t}+\frac{\partial(\rho k u_i)}{\partial x_i}=\frac{\partial}{\partial x_j}\left[\left(\mu+\frac{\mu_t}{\sigma_k}\right)\frac{\partial k}{\partial x_j}\right]+G_k+G_b-\rho\varepsilon-Y_M+S_k$$

$$\frac{\partial(\rho \varepsilon)}{\partial t}+\frac{\partial(\rho \varepsilon u_i)}{\partial x_i}=\frac{\partial}{\partial x_j}\left[\left(\mu+\frac{\mu_t}{\sigma_\varepsilon}\right)\frac{\partial \varepsilon}{\partial x_j}\right]+C_{1\varepsilon}\frac{\varepsilon}{k}(G_k+C_{3\varepsilon}G_h)-C_{2\varepsilon}\rho\frac{\varepsilon^2}{k}+S_\varepsilon \quad \ldots(1)$$

In the model, the turbulent dissipation rate ε is defined as:

$$\varepsilon=\frac{\mu}{\rho}\overline{\left(\frac{\partial u_i'}{\partial x_k}\right)\left(\frac{\partial u_j'}{\partial x_k}\right)} \quad \ldots(2)$$

Turbulent viscosity μ_t can be expressed as a function of k and ε as follows:

$$\mu_t=\rho C_\mu\frac{k^2}{\varepsilon} \quad \ldots(3)$$

Where G_k is the generation term of the turbulent energy k due to the average velocity gradient, G_b is the generation term of the kinetic energy k caused by buoyancy, Y_M represents the contribution of pulsation expansion in compressible turbulence, $C_{1\varepsilon}$, $C_{2\varepsilon,}$ and $C_{3\varepsilon}$ are the empirical constant, σ_k and σ_ε are the Prandtl numbers corresponding to the kinetic energy k and the turbulent dissipation rate ε, respectively. S_k and S_ε are user-defined source items.

Structure and Geometric Parameters

The PODE model was composed of an inlet, flow channel, and outlet (Fig. 2). The flow channel included pit aperture P(mm), pit depth D(mm), arc angle A(°), bottom height B(mm), and right width C(mm) (Fig. 3a).

The value range of geometric structural parameters of the flow channel was as follows: P was 0.6 mm-1.0 mm, D was 1.0 mm-1.4 mm, A was 85°-95°, B was 0.25 mm-0.45 mm,

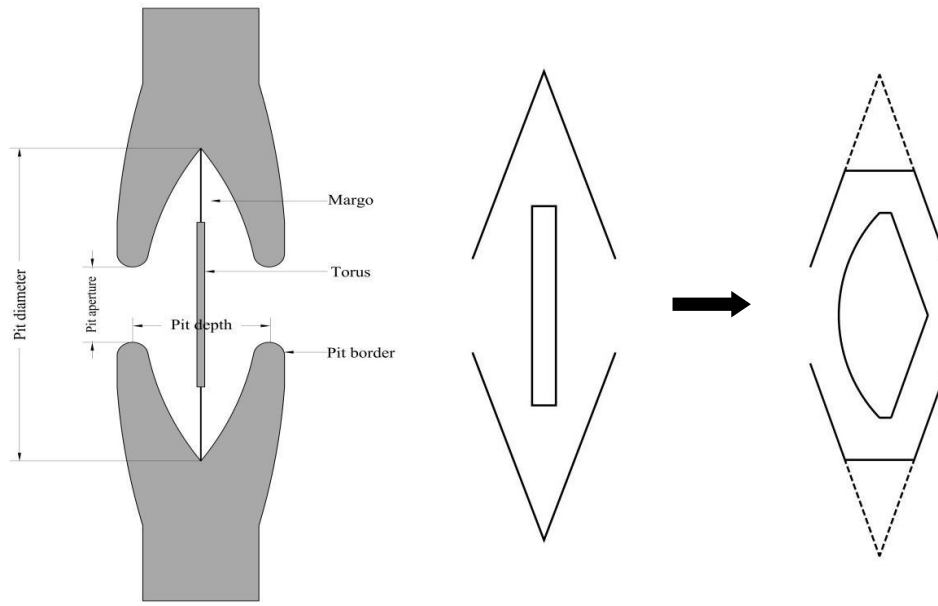

(a) pit structure (b) PDIE (c) PODE

Fig. 1: Schematic diagram of torus-margo bordered pit structure and optimization model.

C was 0.12 mm-0.24 mm. The depth of the PODE model depth was 0.8 mm and the number of channel units was 10.

Meshing and Boundary Conditions

The PODE model was built using SolidWorks software. ANSYS MESH software was used to partition the model fluid domain grid. The unstructured tetrahedron and hexahedron meshes were utilized to mesh the whole channel due to the irregularity of the flow channel. The anticipated pressure drop difference was less than 0.5 percent, and the number of grids had no effect on the calculation findings, according to the prediction accuracy of the input and exit pressure drop. The maximum element size was 0.03 mm, the minimum element size 0.009 mm, and the total mesh number of the flow channel was about 0.38 million. The fluid domain grid is shown in Fig. 3b.

The pressure values for the entrance of the flow channel were set to 50, 75, 100, 125, 150, 175, 200, 225, and 250 kPa, respectively, while the outflow border was set to the outflow boundary. The no-slip condition was applied to the whole channel's wall faces. The computing hardware platform was the five PowerCube-S01 cloud cubes high-performance parallel computers, and the calculation software was ANSYS FLUENT 17.1.

Experimental Model and Scheme

Construction of the Experimental Model

The test rigs were 5 sets of test models. The test PODE structure was connected with the inner wall of the pipe (the contact surface was the front of the PODE). A pressure level set of tests was designed for each time 25 kPa increased within the

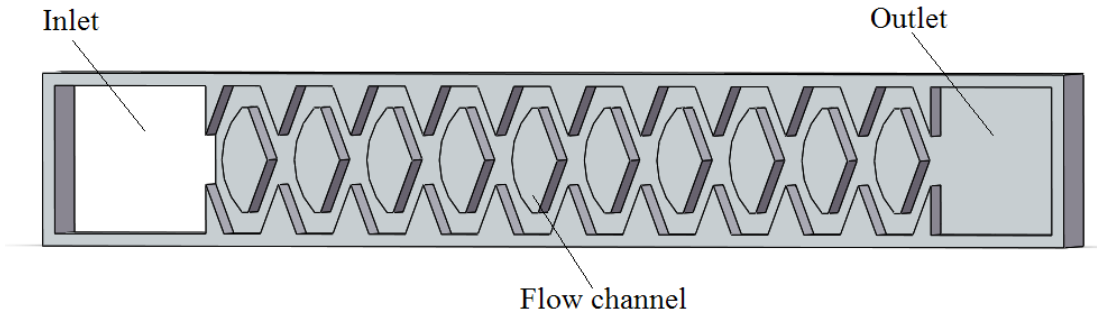

Fig. 2: Schematic diagram of the PODE model.

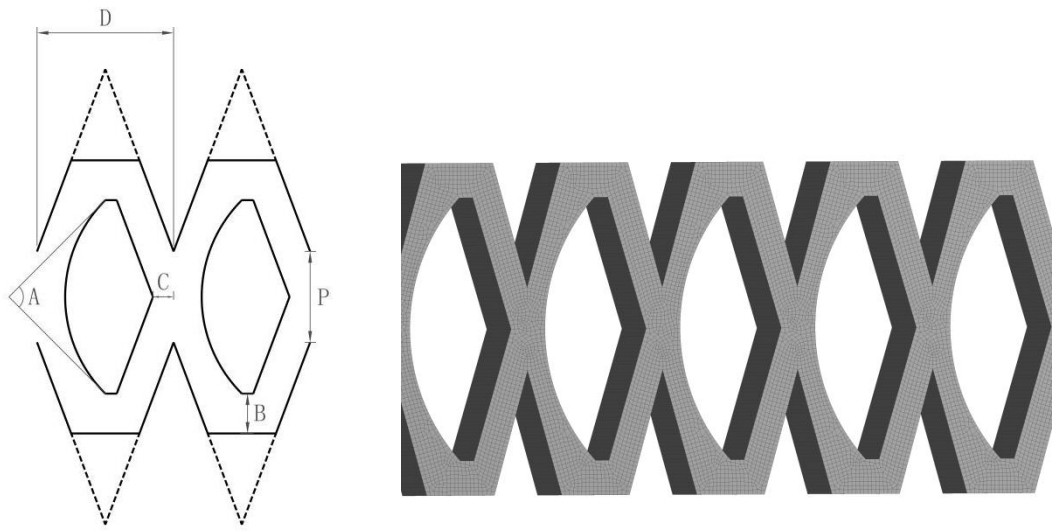

(a) Geometric parameters (b) Fluid domain meshing

Fig. 3: Schematic diagram of the PODE model.

pressure scope range of 50-250 kPa. Each test lasts 15 min, and each pressure level did 3 times of test measurements to take the average values. The flow channel of the PODE was made of plexiglass. A high-precision engraving machine, the EM-G32S-X32, was employed, with a manufacturing precision of 0.01mm and a repeatable positioning accuracy of 0.005 mm. The physical picture of the plexiglass test model is shown in Fig. 4.

Orthogonal Experiment Scheme

The geometry structure parameters of PODE were five factors and five levels (Table 1). The structural schemes of PODE were designed according to the orthogonal experimental design table L25(56). The structural parameter scheme is shown in Table 2.

Calculation Method of Energy Loss Coefficient and Flow Index

The model can be used to examine the fluid flow in a pit structure optimized drip irrigation emitter using the energy conservation law (Bernoulli equation) (Fig. 5). Assuming that the flow between arbitrary sections satisfies the Bernoulli equation, which was written in sections from the inlet to the exit sections Z_1, Z_2, Z_n as :

$$\frac{P_1}{\rho g}+\frac{V_1^2}{2g}+z_1=\frac{P_2}{\rho g}+\frac{V_2^2}{2g}+z_2+\xi_1\frac{V_2^2}{2g}+\lambda\frac{l_1V_2^2}{2Dg}$$
$$\frac{P_2}{\rho g}+\frac{V_2^2}{2g}+z_1=\frac{P_3}{\rho g}+\frac{V_3^2}{2g}+z_3+\xi_2\frac{v_3^2}{2g}+\lambda\frac{l_2V_3^2}{2Dg}$$
$$\cdots\cdots$$
$$\cdots\cdots$$
$$\frac{P_{n-1}}{\rho g}+\frac{V_{n-1}^2}{2g}+z_{n-1}=\frac{P_n}{\rho g}+\frac{V_n^2}{2g}+z_n+\xi_{n-1}\frac{V_n^2}{2g}+\lambda\frac{l_{n-1}V_n^2}{2Dg} \quad \ldots(4)$$

Where P_n and V_n are the average pressure and flow velocity at section n, ρ is the fluid density, g is the acceleration of gravity, z_n is the position head of water at the section, ξ_{n-1} is the local loss coefficient of section *n-1* to section *n,* λ is the friction factor of head loss, l_{n-1} is the length between two adjacent sections, D is the hydraulic radius of the rectangular section flow channel, a and b are the width and depth of the flow channel section, the expression of D is:

$$D=\frac{A}{\chi}=\frac{ab}{2(a+b)} \quad \ldots(5)$$

Table 1: Geometry parameters values of the flow channel.

Level	Geometry parameters values				
	P.mm^{-1}	D.mm^{-1}	A.°$^{-1}$	B.mm^{-1}	C.mm^{-1}
1	0.6	1.0	85	0.25	0.12
2	0.7	1.1	87.5	0.30	0.15
3	0.8	1.2	90	0.35	0.18
4	0.9	1.3	92.5	0.40	0.21
5	1.0	1.4	95	0.45	0.24

Note: P is the distance of pit aperture (mm); D is the distance of pit depth (mm); A is the arc angle of the torus (°); B is the distance of bottom height (mm); C is the distance of right width (mm).

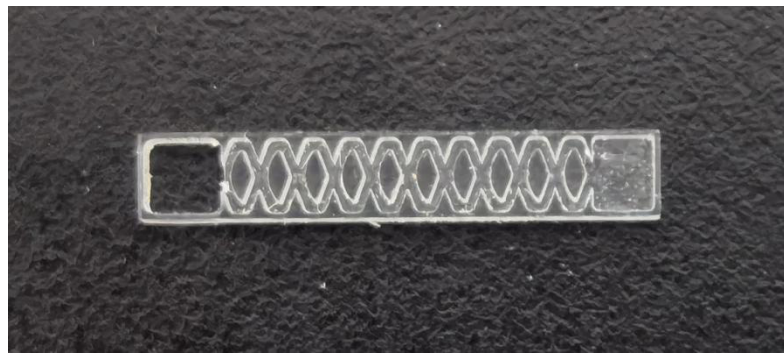

Fig. 4: Prototype of PODE models.

Add the two sides of the equations of Eq. (4) so that:

$$\frac{P_1 - P_n}{\rho g} = z_n - z_1 + \xi_1 \frac{V_2^2}{2g} + \xi_2 \frac{V_3^2}{2g} + \cdots + \xi_{n-1} \frac{V_n^2}{2g} + \lambda \frac{L V_n^2}{2Dg} \quad \ldots(6)$$

Where $l_1+l_2+l_3+\cdots+l_{n-1}=L$, L is the total length of the flow channel. Positioning head due to the horizontal flow path, so $Z_1=Z_2=Z_3=\cdots=Z_n$.

Known by the continuity equation:

$$V_1 A_1 = V_2 A_2 = V_3 A_3 = \cdots = V_n A_n \quad \ldots(7)$$

In Eq. (7), $A_i(i=1,2...,n)$ is the flow area at the corresponding section, substituting Eq. (7) into Eq. (6) we get:

$$\frac{\Delta P}{\rho g} = \left[\lambda \left(\frac{A_1}{A_n} \right)^2 \frac{L}{D} + \sum_{i=1}^{n-1} \xi_i \left(\frac{A_1}{A_{i+1}} \right)^2 \right] \frac{V_1^2}{2g} \quad \ldots(8)$$

Table 2: Orthogonal experiment scheme of the flow channel.

Level	Geometry parameters values				
	P.mm^{-1}	D.mm^{-1}	A.$^{o-1}$	B.mm^{-1}	C.mm^{-1}
1	0.6	1.0	85	0.25	0.12
2	0.6	1.1	87.5	0.30	0.15
3	0.6	1.2	90	0.35	0.18
4	0.6	1.3	92.5	0.40	0.21
5	0.6	1.4	95	0.45	0.24
6	0.7	1.0	87.5	0.35	0.21
7	0.7	1.1	90	0.40	0.24
8	0.7	1.2	92.5	0.45	0.12
9	0.7	1.3	95	0.25	0.15
10	0.7	1.4	85	0.30	0.18
11	0.8	1.0	90	0.45	0.15
12	0.8	1.1	92.5	0.25	0.18
13	0.8	1.2	95	0.30	0.21
14	0.8	1.3	85	0.35	0.24
15	0.8	1.4	87.5	0.40	0.12
16	0.9	1.0	92.5	0.30	0.24
17	0.9	1.1	95	0.35	0.12
18	0.9	1.2	85	0.40	0.15
19	0.9	1.3	87.5	0.45	0.18
20	0.9	1.4	90	0.25	0.21
21	1.0	1.0	95	0.40	0.18
22	1.0	1.1	85	0.45	0.21
23	1.0	1.2	87.5	0.25	0.24
24	1.0	1.3	90	0.30	0.12
25	1.0	1.4	92.5	0.35	0.15

Where,

$$\xi = \left[\lambda \left(\frac{A_1}{A_n} \right)^2 \frac{L}{D} + \sum_{i=1}^{n-1} \left(\frac{A_1}{A_{i+1}} \right)^2 \xi_i \right] \quad \ldots(9)$$

Eq. (8) is simplified to:

$$\frac{\Delta P}{\rho g} = \xi \frac{V_1^2}{2g} \quad \ldots(10)$$

Expressed as:

$$\xi = \frac{2}{V_1^2} \cdot \frac{\Delta P}{\rho} \quad \ldots(11a)$$

Expressed by flow rate:

$$\xi = \frac{2a^2 b^2}{q^2} \cdot \frac{\Delta P}{\rho} \quad \ldots(11b)$$

In Eq. (11a, b), ξ is the flow channel energy loss coefficient (frictional head loss and local head loss), q is the average flow rate of the flow channel. Obviously, ξ reflects the energy dissipation capacity of pit structure optimized drip irrigation emitter flow channel. The expression of q is:

$$q = kH^x \quad \ldots(12)$$

Where k is the flow coefficient; H is the inlet pressure, kPa; x is the flow index.

RESULTS AND DISCUSSION

Flow-Pressure Relationship and Flow Index of Flow Channel

The numerical simulation results of the orthogonal experiment are shown in Table 3. Formula (12) is used to fit the relationship between flow and pressure. The coefficient of determination was 0.996-0.999, and the regression equation had a good correlation. The flow index of different geometric parameters ranged from 0.4632 to 0.5265. Taking experiment schemes 21 and 22 as the example (Fig. 6), the root mean square error between the fitted value and the experimental value is 0.005 and 0.008 L.h^{-1}, which more accurately reflects the relationship between the pressure and flow of the PODE.

Energy Loss Mechanism and Velocity Distribution

The energy loss effect of the flow channel was solved by the Bernoulli equation (11b). The results showed that the energy loss coefficient of the channel structure was 510-2221 at 5-15 m in the 25 experiment schemes (Table 4), which showed that the energy loss effect was obvious.

Take scheme 1 (maximum energy loss coefficient) and scheme 15 (minimum energy loss coefficient) under 50kpa pressure as an example. The fluid velocity at all points in

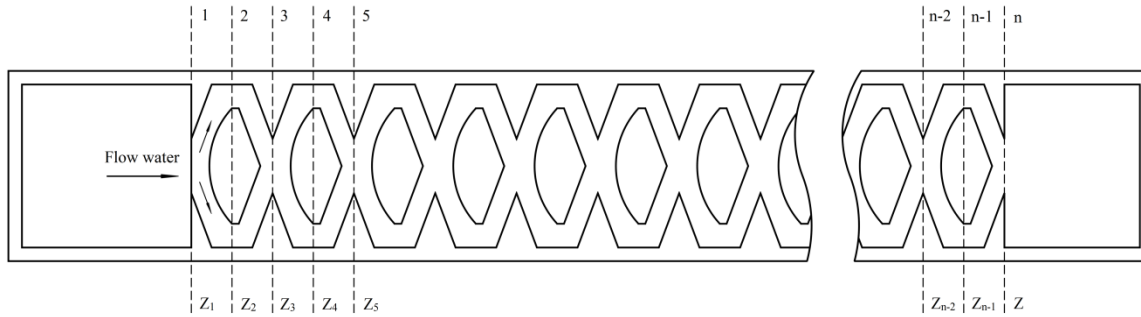

Fig. 5: Schematic diagram of water flow in PODE flow channel.

the flow channel was not the absolute flow velocities in the PODE (Fig. 7). The comparing velocities within different sites in the flow channel, on the other hand, were accurate. The arc structure on the left side of the torus caused the fluid

Table 3: Orthogonal experiment numerical simulation results.

Level	Flow rate q. $L{\cdot}h^{-1}$	Flow coefficient	Flow index	Level	Flow rate q. $L{\cdot}h^{-1}$	Flow coefficient	Flow index
1	1.467	0.1863	0.5265	14	2.685	0.3937	0.4914
2	1.890	0.2573	0.5112	15	3.049	0.4416	0.4942
3	2.269	0.3330	0.4925	16	1.611	0.2531	0.4735
4	2.542	0.3748	0.4899	17	1.987	0.2909	0.4918
5	2.77	0.4073	0.4904	18	2.519	0.3880	0.4778
6	1.694	0.2403	0.4989	19	2.818	0.4279	0.4813
7	2.017	0.3160	0.4735	20	2.596	0.3729	0.4964
8	2.396	0.3499	0.4919	21	1.798	0.2929	0.4632
9	2.280	0.3120	0.5102	22	2.206	0.3494	0.4705
10	2.796	0.3931	0.5028	23	2.163	0.3292	0.4814
11	1.840	0.2886	0.4734	24	2.631	0.3927	0.4870
12	1.760	0.2435	0.5056	25	2.998	0.4350	0.4933
13	2.152	0.3236	0.4854				

Note: q, flow rate value under inlet pressure 50 kPa; Flow index is estimated by the regression model.

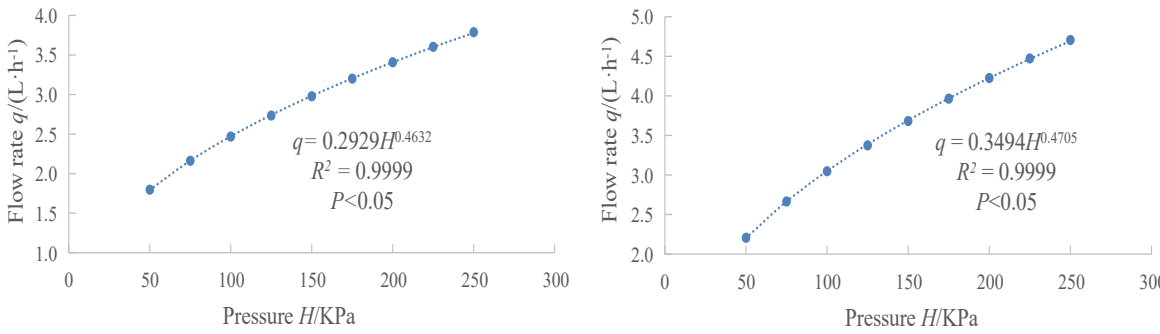

(a) experiment scheme 21 (b) experiment scheme 22

Fig. 6: Relationship between flow rate and pressure for test schemes 21 and 22.

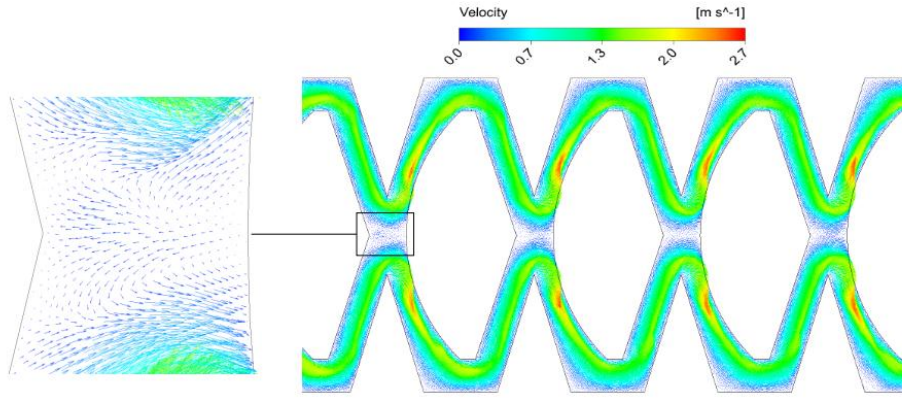

(a) Experimental scheme 1

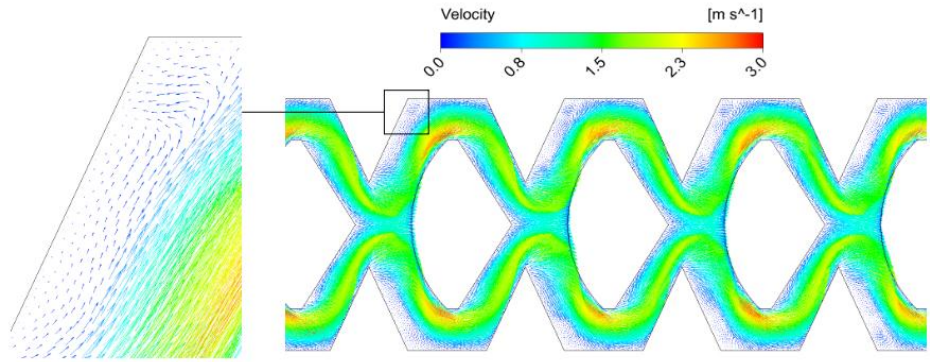

(b) Experimental scheme 15

Fig. 7: Relationship between flow rate and pressure for experimental schemes 1 and 15.

Table 5: Range analysis results for orthogonal experiment.

Scheme	Flow index					
	Level	P.mm^{-1}	D.mm^{-1}	A.$^{\circ-1}$	B.mm^{-1}	C.mm^{-1}
Ki value	1	2.5105	2.4355	2.4690	2.5201	2.4914
	2	2.4773	2.4526	2.4526	2.4599	2.4659
	3	2.4500	2.4290	2.4290	2.4679	2.4454
	4	2.4208	2.4598	2.4542	2.3986	2.4411
	5	2.3954	2.4771	2.4410	2.4075	2.4102
Ki avg value	1	0.5021	0.4871	0.4938	0.50402	0.49828
	2	0.49546	0.49052	0.49052	0.49198	0.49318
	3	0.49000	0.48580	0.48580	0.49358	0.48908
	4	0.48416	0.49196	0.49084	0.47972	0.48822
	5	0.47908	0.49542	0.48820	0.48150	0.48204
Best level		1	5	1	1	1
R		0.0230	0.0096	0.0080	0.0243	0.0162
Number of levels		5	5	5	5	5
Number of repeats per level r		5	5	5	5	5

Note: Ki is the sum of the flow index for level i; Ki avg is the arithmetic mean of Ki

coming into the pit aperture to flow up and down at both ends, resulting in two high-speed areas at the arc boundary. The complete low-speed vortex is not observed in Fig. 7. The junction of the two units in scheme 1 and the upper and lower boundaries on the left side of the unit in scheme 2 produced low-speed mixing. It was discovered that the energy loss impact of the PODE model was related to the flow rate and velocity distribution by combining the flow velocity distribution and geometric structural factors. The low-flow PODE model in the mixing area at the unit connection had a better energy loss effect.

Influencing Factors of Flow Index

Based on the range analysis of the flow index simulation values (Table 3), the results are shown in Table 5. The range value showed that the order of the influence of each geometric parameter on the flow index was B>P>C>D>A. The optimal solution was $P_{0.6}D_{1.4}A_{85}B_{0.25}C_{0.12}$.

Further analysis of the trend of the relationship between each parameter and the flow index (Fig. 8), it can be seen that the flow index decreases with the increase of P, A, B, and C, and increases with the increase of D.

The analysis of variance (Table 6) showed that the corresponding P-value of factor B is less than 0.05, which had a significant influence on the flow index, while the factors P, D, A, and C have no significant influence on the flow index.

Establishment and Verification of Flow Index Prediction Model

Based on the results of the orthogonal experiment, SPSS software was used to perform a multiple linear regression with a confidence level of 95%, and the regression model between the flow index and each parameter was calculated as

$$x = 0.6265 - 0.0573P + 0.0181D - 0.0006A - 0.1146B - 0.1248C \quad \ldots(13)$$

The regression coefficient significance test F statistic value of this model was 21.144, the coefficient of determination R2 was 0.85, the significance level Sig.=0.000, the regression effect was significant, and the established regression equation was valid.

To further verify the reliability of the regression model, three groups of different sizes were selected within the range of geometric parameters (Table 7), and the model samples were processed for testing, the simulation values and test values of the flow index, and the estimated values of the regression model were showed in Table 7. The calculation showed that the relative error of the flow index was -1.80% to 1.29%, which was less than 5%, indicating that the regression model of formula (13) can accurately reflect the quantitative relationship between the flow index and the geometric parameters of the flow channel. The formula (13) can be used to pre-research and evaluate the flow index of this type of drip irrigation emitter, which improved the effectiveness of the drip irrigation emitter test arrangement to a certain extent.

CONCLUSION

(1) The geometric parameter design of the OSPE was carried out. The flow index obtained by the orthogonal experiment was 0.4632-0.5265, indicating that

Table 6: Variance analysis of the effect of geometric parameters on flow index.

Variance source	Sum of square	Degree of freedom	Mean sum of square	F Value	P-Value
P	0.0016	4	0.0004	2.4511	0.0794
D	0.0003	4	0.0001	0.3153	0.8643
A	0.0003	4	0.0001	0.3153	0.8643
B	0.0020	4	0.0005	3.2037	0.0347
C	0.0007	4	0.0002	0.8528	0.5087

Table 7: Verification scheme and results.

Level	Geometry parameters values					Flow index			Error/%	
	P.mm^{-1}	D.mm^{-1}	A.° $^{-1}$	B.mm^{-1}	C.mm^{-1}	Simulation value	Test value	Estimated value	S/E	T/E
1	0.6	1.0	90	0.40	0.21	0.4905	0.4898	0.4842	1.29%	1.14%
2	0.8	1.2	92.5	0.30	0.15	0.4965	0.4905	0.4938	0.55%	-0.67%
3	0.9	1.4	87.5	0.25	0.12	0.4988	0.4953	0.5042	-1.07%	-1.80%

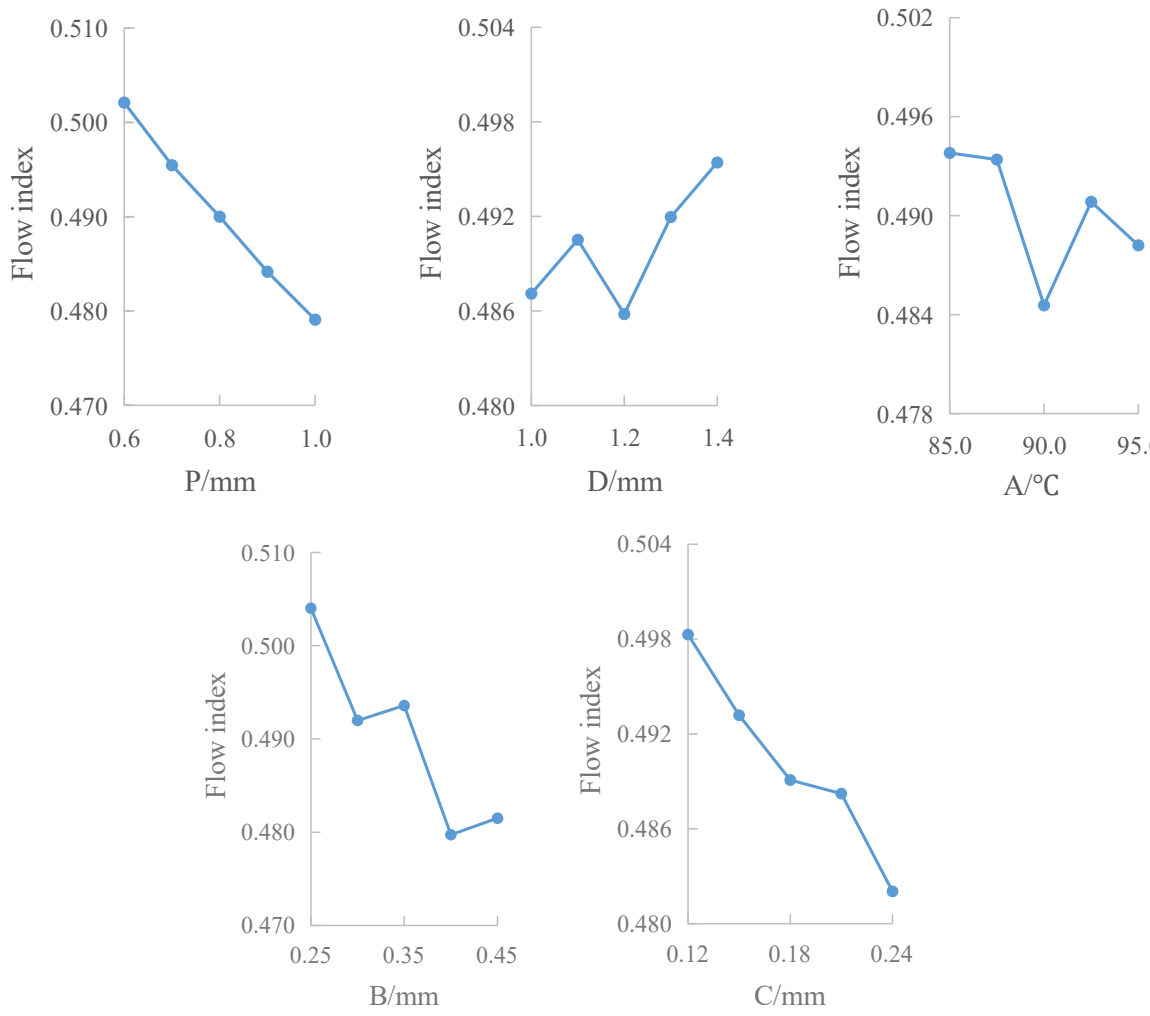

Fig. 8: Effect of geometric parameter on flow index.

its hydraulic performance was good. The energy loss coefficient under the pressure head of 5-15 m was 510-2221. Compared with the traditional unit flow channel structure, the energy loss effect was significantly improved, indicating that the structure of this type of drip irrigation emitter was reasonable and has application prospects.

(2) There was no low-speed vortex zone in the model flow channel, and the anti-clogging performance was good. The results showed that the flow index decreased with the increase of P, A, B, and C, and increased with the increase of D. B had a significant effect on the flow index, while the other parameters had no significant effect on the flow index. The influence order of the geometric parameters on the flow index was B>P>C>D>A, The optimal solution was $P_{0.6}D_{1.4}A_{85}B_{0.25}C_{0.12}$.

(3) The flow index prediction model was established, and the relative error among the test value, simulated value, and estimated value was less than 5%, which proved the accuracy and reliability of the regression model.

ACKNOWLEDGEMENT

This work was supported by the Basic Scientific Research Fund of Heilongjiang Provincial Universities: (2021-KYY-WF-0050).

REFERENCES

Barthlott, W., Mail, M., Bhushan, B. and Koch, K. 2017. Plant surfaces: structures and functions for biomimetic innovations. Nano-Micro Lett., 9(23): 1-40.

Feng, J., Li, Y., Wang, W. and Xue, S. 2018. Effect of optimization forms of flow path on emitter hydraulic and anti-clogging performance in the drip irrigation system. Irrig. Sci., 36: 37-47.

Koch, K., Bhushan, B. and Barthlott, W. 2009. Multifunctional surface structures of plants: an inspiration for biomimetics. Prog. Mater. Sci., 54(2): 137-178.

Guo, L., Bai, D., Wang, X. and He, J. 2016 Analysis of working mechanism and hydraulic performance of two-way flow channel stabilizer in bubbler irrigation emitter. J. Drain. Irrig. Mach. Eng., 34(3): 270-276.

Luo, Y., Liu, W., Li, W. and Xie, W. 2016. Heat and mass transfer characteristics of leaf-vein-inspired microchannels with wall thickening patterns. Int. J. Heat Mass Transf., 101: 1273-1282.

Lu, H., Kang, S., Du, T., Ling, T., Ding, R. and Li, S. 2018. Current status and future research trends on water-saving high-efficiency and eco-friendly agriculture. J. Agric., 8(1): 155-162.

Li, J., Bai, D., Wang, X. and Guo, L. 2020. Geometric parameters design and experimental study on new type drip emitter. J. Drain. Irrig. Mach. Eng., 38(1): 95-101.

Li, Y., Yang, P. and Ren, S. 2007. Effects of fractal flow part designing and its parameters on emitter hydraulic performance. Chin. J. Mech. Eng., 43(7): 109-114.

Li, Y., Yang, P., Xu, T., Liu, H., Liu, H. and Xu, F. 2009. Hydraulic property and flow characteristics of three labyrinth flow paths of drip irrigation emitters under micro-pressure. Trans. ASABE, 52(4): 1129-1138.

Mohamed, A.M. and Ahmed, I.A. 2017. Gene expression programming approach for modeling the hydraulic performance of labyrinth-channel emitters. Comp. Electr. Agric., 142: 450-460.

Sun, J.S. and Kang, S.Z. 2000. The present situation of water resources usage and developing countermeasures of water-saving irrigation in China. Trans. Chin. Soc. Agric. Eng., 16(2): 1-5.

Tian, J., Bai, D., Yu, F. and Guo, L. 2014. Numerical simulation of hydraulic performance on bidirectional flow channel of drip irrigation emitter using Fluent. Trans. Chin. Soc. Agric. Eng., 30(20): 65-71.

Wei, Z., Yuan, W., Zhou, X. and Zhao, G. 2014. Research progress of pressure compensating emitters in micro-irrigation systems in China. Trans. Chin. Soc. Agric. Mach., 45(1): 94-101.

Xing, D., Chen, W., Zhao, L. and Ma, J. 2012. Structural bionic design for high-speed machine tool working table based on distribution rules of leaf veins. Sci. China Technol. Sci., 55(8): 2091-2098.

Xing, S., Wang, Z., Zhang, J., Liu, N. and Zhou, B. 2021. Simulation and verification of hydraulic performance and energy dissipation mechanism of perforated drip irrigation emitters. Water, 13(2): 171.

Xu, T. and Zhang, L. 2019 Hydraulic performance and energy dissipation effect of pit structure flow channel emitter, IFAC. Papers Online, 52(30): 143-148.

Xu, T. and Zhang, L. 2020 Influence and analysis of structure design and optimization of a pit drip irrigation emitter on the performance. Irrig. Drain., 69(4): 633-645.

Yuan, W., Wei, Z., Chu, H. and Ma, S. 2014 Optimal design and experiment for divided-flow emitter in drip irrigation. Trans. Chin. Soc. Agric. Eng., 30(17): 117-124.

Yu, L., Li, N., Liu, X., Yang, Q., Li, Z. and Long, J. 2018. Influence of dentation angle of labyrinth channel of drip emitters on hydraulic and anti-clogging performance. Irrig. Drain., 68: 256-267.

Zhang, S., Zhou, T., Ran, W. and Li, X. 2014 Exploration on internal inlaying drip irrigation pipe and standards. Agric. Sci. Technol., 15(5): 866-869.